

ULRR

Single point and imaging measurements of the optical clearing process

Item Type	Meetings and Proceedings
Authors	Enfield, Joey;O'Doherty, Jim;Leahy, Martin J.
Citation	Novel Optical Instrumentation for Biomedical Applications III;6631/ 66311E
Publisher	Society of Photo-Optical Instrumentation Engineers (SPIE)
Download date	2026-05-15 07:39:39
Item License	https://creativecommons.org/licenses/by-nc-sa/1.0/
Link to Item	https://hdl.handle.net/10344/128

Single point and imaging measurements of the optical clearing process

Joey Enfield, Jim O' Doherty and Martin J. Leahy

Department of Physics, University of Limerick, National Technological Park, Co. Limerick, Ireland

Martin.Leahy@ul.ie

Abstract

Biomedical optics and photomedicine applications are challenged by the turbid nature of most biological tissue systems. This nature limits the penetration depth of light into the tissue. Optical clearing improves the penetration depth of light by the application of optical clearing agents which produce an equalization of refractive indices between tissue components and causes a decrease in tissue scattering, and thus increase in optical transmittance. In this paper we examine the effects of optical clearing agents on *ex vivo* porcine skin using the immersion method. We develop a simple model that can be used to compare different aspects of optical clearing agents such as the rate at which the clearing agents enters the tissue and also the reduction in scattering achieved. We examine the change in the reflected light spectrum over time as the clearing agent enters the skin. This is examined via point probe measurements and also a wide field imaging technique with a consumer-end digital camera. The consumer-end digital camera offers a cheap and simple method for analyzing optical clearing agents over a wider field, overcoming the limitations of single point measurements.

Keywords: Optical Clearing

1. Introduction

Light becomes progressively attenuated as it propagates through tissue due to scattering and absorption from the constituent particles [1]. This limits the depth which light penetrates into the tissue and that at which it becomes randomly scattered. In the visible and near infrared NIR wavelength range scattering is more dominant than absorption [2].

Optical clearing is a technique that causes a decrease in the overall effects of scattering that occurs in tissue by the administration of non-reactive, biocompatible optical clearing agents. Several different methods have been proposed on how these agents reduce the scattering in the tissue. These include equalization of the refractive indices between different tissue components [3, 4, and 5], dehydration [4, 6, and 7] and collagen dissociation [8]; however the most common hypothesis is the refractive indices equalization.

The principle behind the refractive index equalization is that scattering occurs due to refractive index mismatches between different components in the tissue. If the refractive index of the intercellular fluid is matched with that of the tissues structural components there is a reduction in the levels of scattering in the tissue. These agents are chosen such that when they diffuse into the tissue they produce a subsequent outflow of the intracellular fluid which is mainly composed of water under osmotic pressure. The chemicals are also chosen to have a higher refractive index than water which helps reduce the refractive index mismatch that exists between tissue components. This refractive index matching greatly reduces the scattering in the tissue. This process is reversible when upon subsequent immersion in isotonic saline tissue optical and mechanical properties return to their native states [9]

One issue with the use of optical clearing agents is that they also affect the functions of the tissue. They have been reported to lead to temporal local stasis in some blood microvessels of skin [11]. However this affect could be useful for different application as the cessation of blood flow in microvessels can be useful for diagnosis and treatment of diseases [12]. This could offer two advantages, optical clearing and blood flow stopping. It could help to decrease the laser dose required and more effectively destroy abnormal blood vessels during surgical laser treatment of skin vascular diseases [11, 13].

One of the most commonly used clearing agents reported is glycerol however there are many other agents that have been reported throughout the literature; including sorbitol, glucose, trimethylol propane, ethylene glycol, propylene

glycol, trazograph, dextran, dimethyl sulfoxide DMSO. The majority of these clearing agents are benign and biocompatible and many are already in use as sweetening additives in foods and emollients in skin care products.

One of the greatest limitations of optical clearing agents are the methods of application of the agents. The low permeability of skin to most optical clearing agents prevent topical application of optical clearing agents. In recent litterateur [14,15] it has been reported that the combination of different agents could greatly increase the rate that the agent enters into the tissue. Chemical agents such as DMSO (Dimethyl sulfoxide) which penetrate the skin quickly and deeply without damaging the tissue but does not offer a high level of scattering reduction[16], however it could be used as a carrier to carry other chemical agents which offer greater levels of scattering reduction such as glycerol into the tissue. However DMSO can be dangerous if mixed with certain chemicals due to its ability to easily penetrate the skin so oleic acid has also been investigated [17].

2. Theoretical Background.

To understand how the optical clearing process produces a reduction in the scattering in tissue it is necessary to understand how light interacts with tissue. In general, the propagation of light through a thin tissue layer of thickness d is modeled by the Beer-Lambert relationship which states [18,19]

$$I(d) = I_0 e^{-\mu_t d} \quad (\text{Eq. 1})$$

Where $I(d)$ is the intensity that is transmitted, μ_t is the attenuation coefficient and $\mu_t = \mu_a + \mu_s$, where μ_a is the absorption coefficient and μ_s is the scattering coefficient. This shows that the transmission of a beam of light through a tissue layer is related to both the level of scattering in the tissue and the level of absorption. The reduced scattering coefficient μ'_s , is defined as a measure of the number of scattering events required for a population of photons to disperse isotropically throughout a tissue sample. This reduced scattering coefficient is related to the scattering coefficient by

$$\mu'_s \equiv \mu_s (1 - g) \quad (\text{Eq. 2})$$

Where g is a measure of scattering anisotropy. If the tissue is modeled by a simple monodisperse tissue model, this is a model that assume the tissue consist of spherical scatters with equal diameter of $2a$, with a volume fraction given by f_s and refractive index η_s in a background material with a refractive index η_b . The reduced scattering coefficient can be obtained from Mie Theory [18]

$$\mu'_s = 3.28\pi a^2 f_s \left(\frac{2\pi a}{\lambda} \right)^{0.37} \left(\frac{\eta_s}{\eta_b} - 1 \right)^{2.09} \quad (\text{Eq. 3})$$

From Eq. 3 it is clear to see that $\mu'_s \propto \left(\frac{\eta_s}{\eta_b} - 1 \right)^{2.09}$, this means that as the refractive index of the background material approaches the refractive index of the scatters the reduced scattering coefficient reduce i.e. $(\eta_b \rightarrow \eta_s) \Rightarrow (\mu'_s \rightarrow 0)$ when the reduced scattering coefficient is reduced this will reduce the overall scattering in the tissue and the sampling depth in the tissue is increased.

3. Methodology

3.1. Sample Preparation

Samples used were blood free porcine skin which was obtained from a local abattoir. The samples were frozen upon receipt at a temperature of -18°C and all samples were used within 2 week of freezing. Prior to each experiment the samples were allowed to defrost for 1 hour in open air and all the experiments were commenced within 2 hours of defrosting.

The samples were cut into rectangular sections of approximately 2 cm x 8 cm using a sharp razor blade. For each experiment it was required that the samples must be a uniform thickness. A technique that could produce samples with a uniform thickness was developed. The basic apparatus for this is shown in Figure 1

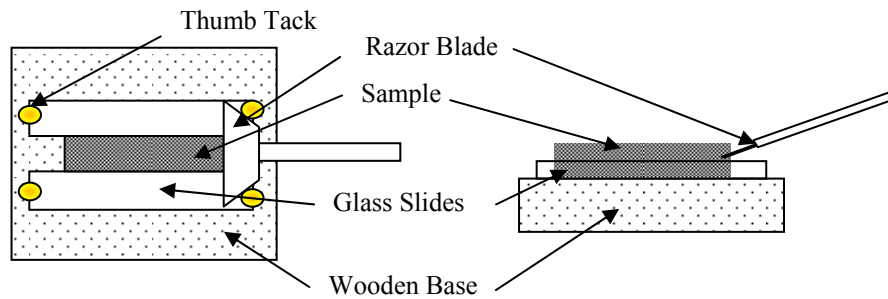


Figure 1: Apparatus used to prepare samples

Firstly a layer of plastic wrap was placed down onto the wooden block; this was done to ensure a clean surface under the sample. The sample was then placed epidermis side down, onto the block. Two glass slides were then placed next to the sample and were held in place with thumb tacks. A razor blade was then used to cut the sample to the required thickness. This was done by sliding it over the glass slides while the sample was held down in place by hand. The sample thickness could be varied by placing more than one glass slide, for small variations in sample thickness sheets of paper could also be placed under the glass slides. This method allowed for uniform samples to be cut with thickness as low as $0.9 \text{ mm} \pm 0.1 \text{ mm}$.

Once the samples had been cut each sample was visually examined to ensure that there was a uniform thickness across the sample. If the sample appeared uniform it was then placed between two glass slides. The thickness of the sample between the two glass slides was then measured using a micrometer; several measurements were taken at random locations across the sample to determine the sample thickness. The thickness of the sample was then obtained by taking the thickness of the two glass slides away from the measured thickness.

3.2. Experimental Apparatus

A basic schematic of the system used in the experiments is shown in Figure 2.

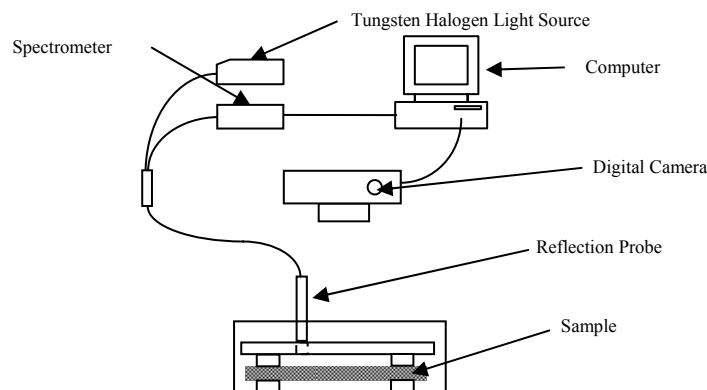


Figure 2: Apparatus used in clearing experiment to capture spectral reflectance data and imaging of the clearing process

The experimental apparatus was designed to allow both the reflected spectrum and imaging of the sample to be recorded as the sample cleared. The imaging was performed via a Canon PowerShot G7 digital camera which comes with software that allows for remote control of the camera via a computer. This software allowed for imaging to be automatic controlled via the computer. The camera was kept at a height of approximately 50 cm above the sample. The focal length of the camera was 22 mm, the aperture setting was $f/3.5$, the exposure time was $1/40\text{s}$ and the ISO was set to 50. The reflected spectrum was measured using a reflected probe system. The probe system consisted of a circular array of 6

optical fibers which had diameters of 200 μm which illuminated the sample with light from Ocean optics LS-1 Tungsten Halogen Light Source. A schematic of the tip of the spectral probe is shown in figure 3

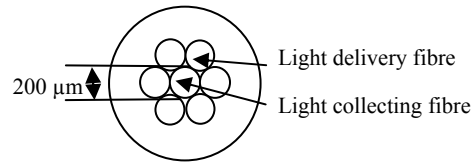


Figure 3: Schematic of Reflection Probe Tip

The reflected light is then collected by a core fiber which carried the reflected spectrum to a Ocean Optics USB-2000 spectrometer; The spectrometer was controlled by OOIBase32 (Ocean Optics) software and simultaneously measured the reflected spectrum on the range 550 nm to 1200 nm every 10 s.

The sample was placed into a specifically designed sample holder. A schematic of the sample holder used in the experiments is shown in Figure 4.

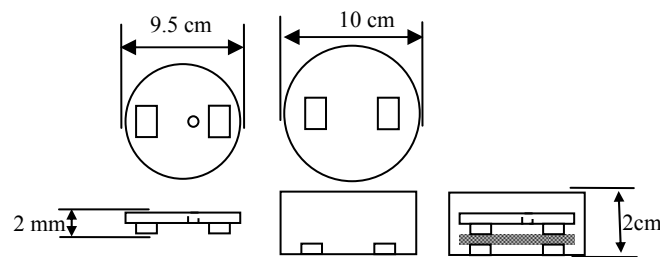


Figure 4: Schematic of Sample Holder

The holder is designed so that the sample could be suspended in a clearing agent and also to hold it in place as it clears. The sample needed to be held in place as it was found that as the clearing agent enters into the sample, the sample begins to shrink. While the sample shrank it had a tendency to bend and this would produce a great change in the point probe reflectance measurements. A hole was also drilled through the top of the sample holder which was just large enough to hold the point probe in place. This was done so that the point probe would be held at a constant height above each sample.

In each experiment the reflected spectrum was recorded at intervals of 10 s. Each measurement consisted of the average of 100 data acquisitions and each data acquisition was acquired for 100 ms. Images of the clearing process were recorded every 5 min. A black card was placed under the sample holder to set a constant background color under all the samples. On this card there was also a set of red, green, blue and white squares which were used as references. This was done as it was found that the camera was automatically attempting to white balance the images. This meant that after each experiment the images had to be processed to remove this white balancing by the camera.

4. Results

4.1. Spectral Probe Results:

In the experiment the reflected spectrum was recorded over time. The spectrometer used was able to measure on a wavelength range from 500 nm to 1200 nm. The light source used in the experiment was not a perfect white source as can be seen from figure 5 (b) which shows the spectrum of the light source used. This meant that a technique to remove the dependence on light source from results were required. This was achieved by normalizing the results. The normalization was performed by dividing the intensity at any time or wavelength by the initial intensity value at that wavelength and is a measure of the fractional change in intensity at any time.

$$N(\lambda, t) = \frac{I(\lambda, t)}{I(\lambda, 0)} \quad (\text{Eq. 4})$$

The typical data that was recorded by the spectral reflectance probe in each experiment as the sampled was cleared is shown in figure 5 (a).

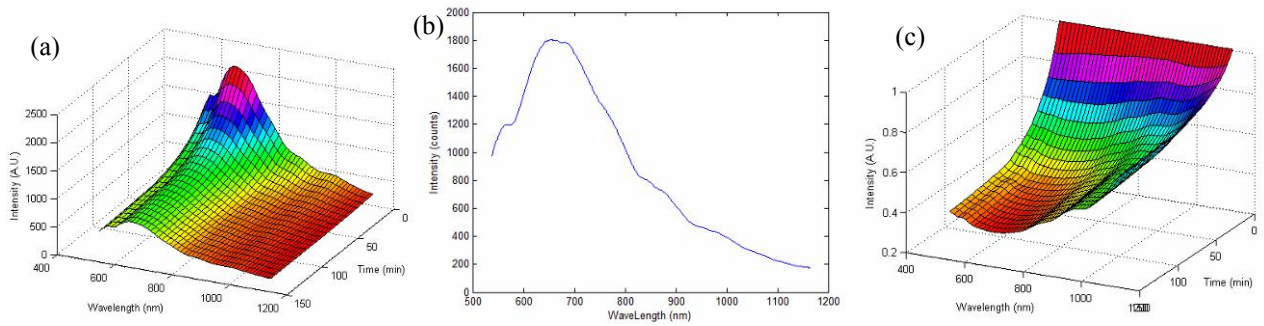


Figure 5 (a) The change in the reflected intensity at various wavelengths as the sample is cleared as recorded by the spectral probe (b) Graph of the tungsten halogen light source spectrum (c) The fractional change in reflected intensity during the clearing process.

Initially there was a large reflected spectrum however as the sample cleared the levels of reflected light dropped by up to 80%. The large peak that is seen in (a) is due to the light source spectrum. To get a better impression of what is occurring normalization of the data using Eq. 4 is shown in figure 5(c). Normalizing the data helps to remove the dependence on the light source.

If a the change in intensity at a single wavelength is examined over time wavelength as shown in figure 6, it is seen that the reflected intensity drops as the clearing agent enters into the tissue. This is occurring as the levels of scattering in the tissues is reducing which is leading to a drop in the levels of backscattered light.

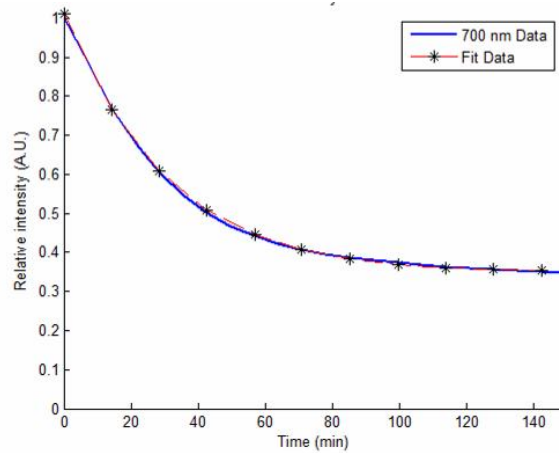


Figure 6 Change in intensity at 700 nm. The graph shows the raw data and also the data fitted to a model

The change in the reflected light intensity over time as the optical clearing agent enters the can be modeled using the following equation

$$N(t, \lambda) = A(\lambda)e^{-bt} + C(\lambda) \quad (\text{Eq. 5})$$

This equation consists of two separate terms, one that is related to the clearing rate and one related to the steady state that is reached. In examining the terms in this equation it is found that the b term controls the rate that the clearing process occurs and could be related to the rate that the optical clearing agent enters the sample. The C term is related to the steady state of clearing that is reached. The equation can be used as a simple system to compare the optical clearing properties of different clearing agents. This is valid provided that the samples used have approximately the same parameters i.e sample thickness, sample pigmentation and that the experiments are carried out under similar condition i.e probe height, temperature, sample stage. This equation then allows for a method that can be used to qualify the effectiveness of optical clearing agents without the expenses and difficulty involved in using tools such as integrating spheres.

4.2. Imaging Results

While working with the point probe system many shortcomings with the using point probes quickly came to light. It was found that slight movements in the sample would have a great effect on the results measured. As the samples cleared they would shrink as the clearing agents entered the tissue. This could cause the sample to bend which would greatly affect the point probe results. It was also found that if the point probe was placed above a hair follicle or a follicle passed under the probe as the sample was clearing that it could also affect the results. These effects would show up as an increase in the reflected spectrum.

To overcome these limitations an imaging system was used. The basic principle behind the technique is that if a known background is behind a sample, as the sample begins to clear the background color will begin to show through. Examining this change in the pixel values as the sample clears from the sample color to the background color can give information about the clearing process.

The imaging was carried out using a standard home user digital camera which introduced many issues with the results. It was found that the camera would attempt to auto white balance successive images. This meant that the RGB pixel value of the same region would change in successive images. In an attempt to compensate for this a simple balancing algorithm was devised.

Image Balancing Algorithm

This algorithm works by taking a region that should not change color throughout the experiment. The average pixel

value P_{avg}^i of this region in the initial is then calculated by

$$P_{avg}^i = [R^i, G^i, B^i]$$

Where R^i, G^i, B^i are the average values of the red, green, blue pixels in the region. If the same region is then analyzed in the nth images and the average pixel value of the region is again calculated where

$$P_{avg}^n = [R^n, G^n, B^n]$$

The difference in the average pixel value in this region between the initial image and the nth image is then calculated by

$$\Delta P^n = [\Delta R^n, \Delta G^n, \Delta B^n] = P_{avg}^n - P_{avg}^i = [R^n - R^i, G^n - G^i, B^n - B^i]$$

The image is balanced by shifting every pixel in the nth image by this difference:

$$P_{bal}^n(x, y) = [R^n(x, y) - \Delta R^n, G^n(x, y) - \Delta G^n, B^n(x, y) - \Delta B^n] \quad (\text{Eq. 8})$$

Where $P_{bal}^n(x, y)$ is the balanced pixel value at the point x, y in the image. The effects of this balancing are shown in figure 7.

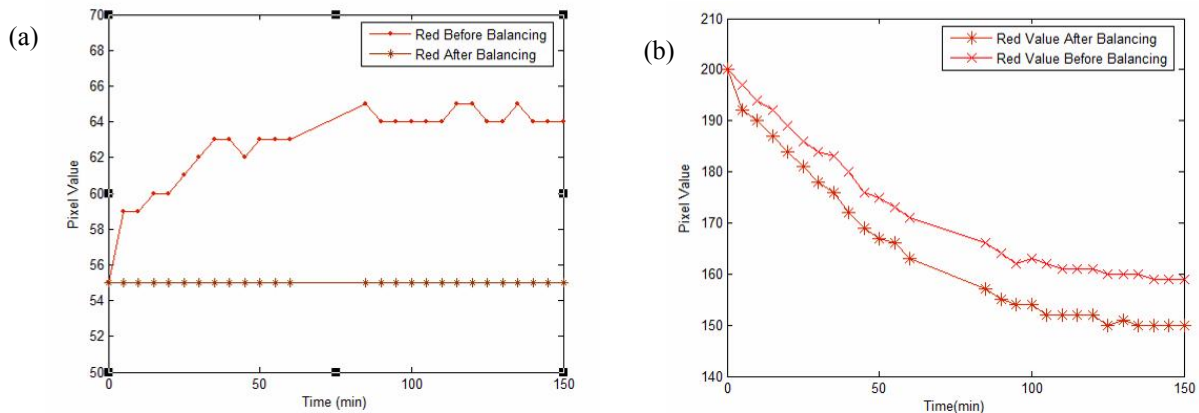


Figure 7. Change in the red pixel value during the clearing process for (a)the static background and (b)a region that is clearing before and after the balancing algorithm is applied.

Figure 7(a) shows the change in the red pixel value that occurred in successive images of the static black background before and after a balancing algorithm was applied. Similar results are seen in each of the pixel planes (Green, Blue). If the RGB value of the images is analyzed as the sample is cleared there can be up to a 10% difference between the RGB values of the balanced images and the unbalanced images; Figure 7 (b) shows the typical results obtained for the red pixel value for a clearing sample, the difference between balancing and unbalanced data can clearly be seen.

4.2.1. Calculating the Normalized Intensity

An issue when working with imaging is determining a suitable algorithm to calculate the normalized intensity from pixels values. If the normalized intensity $N(x, y, n)$ at a point x, y in the n^{th} image calculated by dividing each pixel value P_{bal}^n by the value of the pixel in the initial image $P_{bal}^{n=1}$ i.e.

$$N(x, y, n) = \frac{P_{Bal}^n(x, y)}{P_{Bal}^{n=1}(x, y)} \quad (\text{Eq. 7})$$

It was found that the calculated change in pixel values obtained was too high. The problem with using Eq. 8 is that the background pixel value $P_{background}$ not reaching $[0, 0, 0]$ has to be taken into account. This can be seen in figure 8 which shows the change in the red pixel value for a region of the background value and a region on the sample that is being cleared. An improved method of calculating the normalized intensity was determined to be

$$N(x, y, n) = \frac{P_{Bal}^n(x, y) - P_{Background}}{P_{Bal}^{n=1}(x, y) - P_{Background}} \quad (\text{Eq. 8})$$

This improved method of calculating the normalized intensity showed a much greater change as the sample is cleared as can be seen in figure 8 (b). The figure shows the normalized intensity calculated using both Eq. 7 (without background) and Eq. 8 (with background). It can be clearly seen that Eq. 8 shows a larger change in intensity.

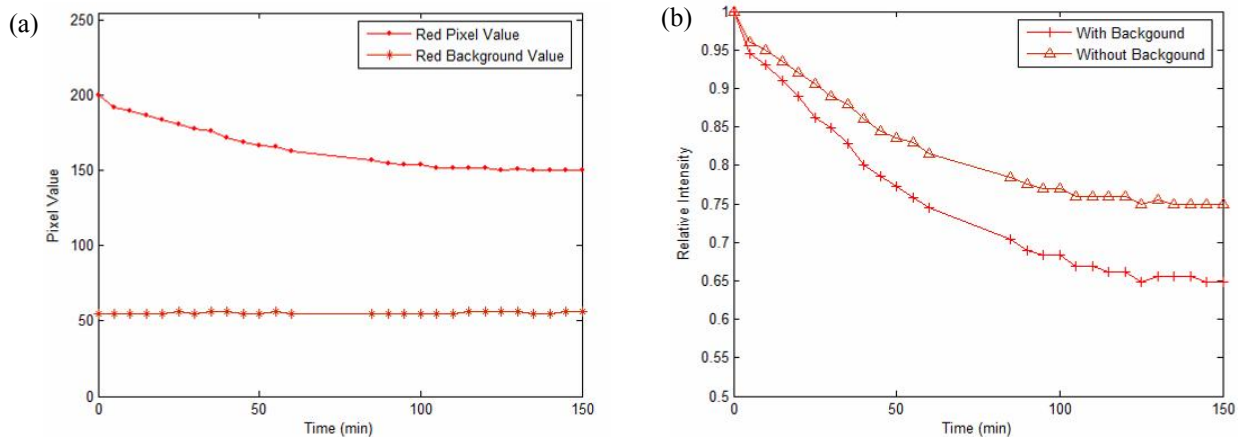


Figure 8 (a) Change in the red pixel value as the sample clears for both a region in the background and on the sample. (b) Normalized intensity of the cleared section without the background color taken into account and with the background color taken into account

This data can then be fitted with Eq. 5 as done with the spectral data. These parameters can then be used to analyze different aspects of the clearing process. Some of the results that have been achieved using this technique are shown in figure 9.

The following results were obtained from running several experiments and obtaining fit data from Eq. 5. The fit parameters a, b, c were then obtained using Matlab 6.5 curve fitting toolbox and the average values from all the

experiments was then taken. The graphs shows in figure 9 were plotted using Eq. 5 with the average values for a, b, c calculated from all the experiments.

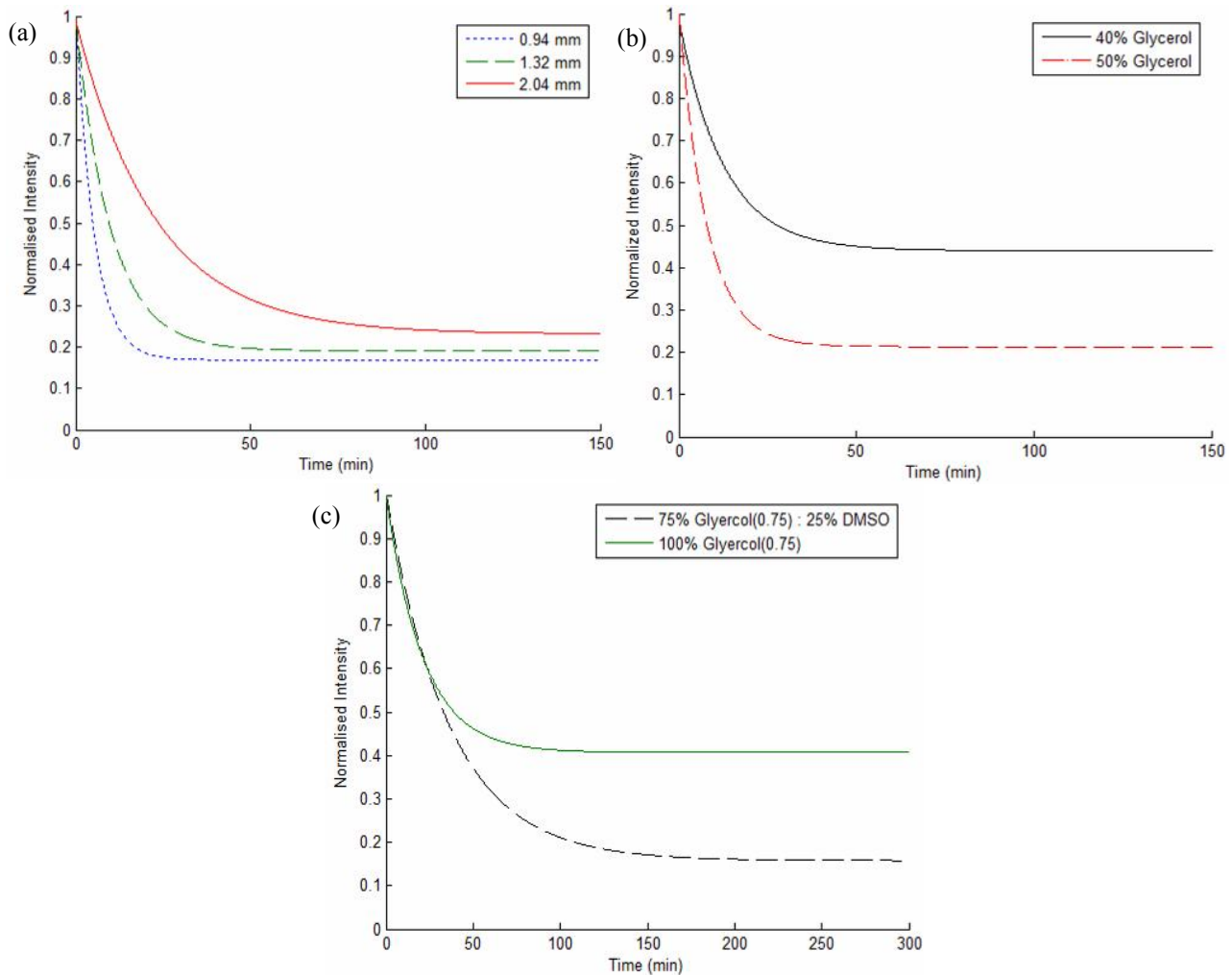


Figure 9 Results Obtained to data using the system. (a)Effect of changing the sample thickness used (b) Effect of changing the clearing agent concentration (c) Effect of using Dimethyl sulfoxide(DMSO) mixed with glycerol

Figure 9 (a) show how varying the sample thickness increases the length of time it takes for the clearing agent to clear the tissue fully, The solution used in each of these experiments was a 50% Glycerol mixed by volume with 50% Demonized water. It also shows how the rate that the clearing agent enters the tissue changes with different sample thickness. The experiment also shows how the level of clearing decreases as the thickness of the samples increase. These experiments shows that the sample thickness should be kept constant when trying to compare data as a small change in the sample thickness of 0.4 mm can almost double the time it takes for the sample to clear.

Figure 9 (b) Shows the effect of varying the concentration of the glycerol solution on the clearing process. The thickness of the samples used in these experiments was approximately 1.3 mm. This results indicates that the clearing agents entered into the tissue at the approximately the sample rate as they seem to achieve their maximum level of clearing at the same time; however the level of clearing that was achieved by using a 50% solution appeared to be greater than that of a 40% solution. This shows how concentration variations can greatly affect the clearing process.

Figure 9 (c) shows the effect of mixing DMSO with glycerol. The thickness of the sample used in these experiments was 2.2 mm. In this experiment a solution of Glycerol (0.75) means a solution of 75% Glycerol with 25% Saline by

volume. The results in this experiment suggest that that an improved level of clearing can be achieved by mixing DMSO with glycerol.

5. Conclusions

This new technique offers a simple and cheap method for comparing different clearing agents. A simple technique for preparing thin samples down to a thickness of approximately 0.9 mm has also been described. The experimental apparatus described in this experiment would be easily and cheaply reproduced in any lab. The results obtained show how it can clearly show large differences between different agents. Some interesting results have already been shown by the technique such as how the concentration affects the clearing process and also the effect of mixing DMSO and glycerol as a clearing agent. It was found that the imaging results appeared to show the same trends as the spectral probe results. However the techniques did not correspond exactly, the reasons for this are still being investigated. This new technique leads to a lot of future work in examining different aspects of clearing agents.

6. Acknowledgments

This project is funded by the Irish Research Council for Science, Engineering and Technology (IRCSET): funded by the National Development Plan.

7. References

- [1] Cheong W., Prah S., Welch A, "A review of the optical properties of biological tissues," IEEE J. Quantum Electron. 1990; 26: 2166-2185
- [2] Choi B., Tsu L., Chen E., Ishak T., Iskandar S., 'Determination of Chemical Agents Optical Clearing Potential Using In Virto Human Skin', Lasers in Surg. & Medic. 2005; 36: 72-75
- [3] Vargas G., Chan E., Barton J., Rylander H., Welch A., ' Use of an agent to reduce scattering in skin.', Lasers Surg. Med. 1999;24:133-141.
- [4] Wang R., 'Signal degradation by multiple scattering in optical coherence tomography of dense tissue: A Monte Carlo study towards optical clearing of biotissues.' Phys Med Biol 2002;47:2281-2299.
- [5] He Y. , Wang R., 'Dynamic optical clearing effect of tissue impregnated with hyperosmotic agents and studied with optical coherence tomography', J. Biomed. Opt. 2004;9: 200-206
- [6] Xu XQ, Wang RK, Elder JB. Optical clearing effect on gastric tissues immersed with biocompatible chemical agents investigated by near infrared reflectance spectroscopy. J Phys D Appl Phys 2003;36:1707-1713.
- [7] Xu X, Wang RK. The role of water desorption on optical clearing of biotissue: Studied with near infrared reflectance spectroscopy. Med Phys 2003;30:1246-1253.
- [8] Yeh AT, Choi B, Nelson JS, Tromberg BJ. Reversible dissociation of collagen in tissues. J Invest Dermatol., J. Phys. D: Appl. Phys. 2003; 121:1332-1335.
- [9] Wells PB, Yeh AT, Humphrey JD. Influence of glycerol on the mechanical behavior and thermal damage susceptibility of collagenous tissues. IEEE Trans Biomed Eng 2006;53(4): 747-753.
- [11] Vargas G, Readinger A, Dozier S, Welch AJ, "Chemical agents for the reduction of light scattering in tissue: implications for light therapeutic applications," Proceedings SPIE, 4609, 2002.
- [12] Galanzha E, Tuchin E, Solovieva E, Stepanova E, Cheng H, "Skin backreflectance and microvascular system functioning at the action of osmotic agents", J. Phys. D: Appl. Phys. 2003 ;36:1739-1746
- [13] Boergen K P 1977 Lasers in Surgery, Medicine, and Biology Proc. 18
- [14] Xiangqun Xu and Ruikang K Wang, Synergistic effect of hyperosmotic agents of dimethyl sulfoxide and glycerol on optical clearing of gastric tissue studied with near infrared spectroscopy, 2004 Phys. Med. Biol. 49 457-468
- [15] Jingying Jiang^{1,2} and Ruikang K Wang¹ Comparing the synergistic effects of oleic acid and dimethyl sulfoxide as vehicles for optical clearing of skin tissue in vitro Phys. Med. Biol. 49 (2004) 5283-5294
- [16] Bernard Choi, PhD, Determination of Chemical Agent Optical Clearing Potential Using In Vitro Human Skin, Lasers in Surgery and Medicine 36:72-75 (2005)
- [17] Ruikang K., Jiang J. , Comparing the synergistic effects of oleic acid and dimethyl sulfoxide as vehicles for optical clearing of skin tissue in vitro", 2004 Phys. Med. Biol. 49 5283-5294
- [18] Valery V. Tuchin. 2006, Optical Clearing of Tissues and Blood. SPIE publishing p1-50
- [19] Tuan Vo-Dinh, 2000, Biomedical Photonics Handbook, CRC publishing p2.5 - 2.30